Vibration and Stability of a Shallow Arch Under a Moving Mass-Dashpot-Spring System

Jen-San Chen
Professor
e-mail: jschen@ccms.ntu.edu.tw

Min-Ray Yang
Graduate Student

Department of Mechanical Engineering,
National Taiwan University,
Taipei, Taiwan 10617

In this paper we study the dynamic behavior of a shallow arch under a moving load system containing two masses, a dashpot, and a suspension spring. It is assumed that the masses in the load system are under the action of gravity. This paper is an extension of a previous publication in which the arch is loaded by a moving point force. The emphasis of the paper is placed on finding out how the inertia effect of the load system affects the dynamic response of the arch. It is found that the point-force model is a good approximation only when the arch is slender and the moving speed of the load system is low. The boundary of a dangerous speed zone is defined based on the comparison of the total energy gained by the arch and an energy barrier. It is observed that the suspension model predicts a considerably different dangerous speed zone from the one predicted by the point-force model, especially in the high-speed range. [DOI: 10.1115/1.2345673]

Introduction

When a vertical load is applied on a horizontally positioned sinusoidal arch and is increased quasi-statically, axial thrust will develop and grow due to the immovability of the ends. At certain critical load the arch may undergo snap-through buckling [1–9]. In the case when the vertical load is applied suddenly instead of in the quasi-static manner, the phenomenon is dynamic and much more complicated [10–23]. More importantly, the critical load will be different from the one predicted statically. For instance, if a vertical load is applied suddenly, the critical load will be about 80% of the one applied quasi-statically [10].

In all these previous researches, the vertical loading, either distributed or concentrated, is assumed to be fixed in space. In Ref. [24] Chen and Lin studied the dynamic snap-through of a shallow arch under a moving point force. The motivation of their research is to study the speed effect of a moving vehicle on the stability of a public transportation structure which can be modeled as an arch. They reported that when the point load is greater than a critical value there exists a finite speed zone within which the arch runs the risk of dynamic snap-through. In this paper we extend the research in Ref. [24] by replacing the point force by a mass-dashpot-spring system, which is a more realistic model for an operating vehicle. The point-force model in Ref. [24] is a special case of the current one with the coupling effect between the load system and the arch being neglected.

Equations of Motion

Figure 1(*a*) shows an elastic shallow arch under a moving mass-dashpot-spring system containing two masses m_1^* and m_2^*, a dashpot c^*, and a spring k^*. The initial shape of the unloaded arch is $y_0(x)$ with the distance between the two pinned ends being L. The load system is subjected to a horizontal force $F^*(t)$ and travels from $x=0$ to $x=L$ with a constant horizontal speed v^*. The lower mass m_1^* moves up and down along with the vibrating arch while sliding along the arch without friction. The mass m_2^* moves in line with m_1^* vertically. The equation of motion of the loaded arch can be written as

$$\rho A y_{,tt} = -EI(y-y_0)_{,xxxx} + p^* y_{,xx} - Q^* \delta(x - v^* t) \tag{1}$$

The conventional use of comma for partial differentiation is adopted here. $y(x,t)$ is the shape of the deformed arch. For a "shallow" arch we assume that the slope of the neutral axis of the curved beam (before and after deformation) is small compared to 1, or more precisely, $y_{,x}^2 \ll 1$. Under this assumption the curvature of the curved beam can be approximated by $y_{,xx}$. The parameters E, ρ, A, and I are Young's modulus, mass density, area, and moment of inertia of the cross section of the arch. p^* is the induced axial force in the arch

$$p^*(t) = \frac{AE}{2L}\int_0^L (y_{,x}^2 - y_{0,x}^2)dx \tag{2}$$

δ is the Dirac delta function. Q^* is the vertical component of the force applied by the load system on the arch

$$Q^* = m_1^*\left(g + \frac{d^2y_1}{dt^2}\right) + m_2^*\left(g + \frac{d^2y_2}{dt^2}\right) \tag{3}$$

g is the acceleration of gravity. $d^2y_1(t)/dt^2$ and $d^2y_2(t)/dt^2$ are the accelerations of masses m_1^* and m_2^*, respectively, in the vertical direction. It is assumed that the gravity on the arch itself can be neglected by comparison with the weight of the masses. $y_1(t)$ is related to $y(x,t)$ by

$$y_1(t) = y(x = v^* t, t) \tag{4}$$

Therefore by chain rule

$$\frac{d^2y_1(t)}{dt^2} = y_{,tt} + 2v^* y_{,tx} + v^{*2} y_{,xx} \tag{5}$$

The additional equation of motion for mass m_2^* can be written as

$$m_2^*\frac{d^2y_2}{dt^2} + c^*\frac{d(y_2 - y_1)}{dt} + k^*(y_2 - y_1) = 0 \tag{6}$$

The pinned-pinned boundary conditions for y at $x=0$ and L are

$$y(0) - y_0(0) = y_{,xx}(0) - y_{0,xx}(0) = y(L) - y_0(L) = y_{,xx}(L) - y_{0,xx}(L) = 0 \tag{7}$$

It is noted that in order for the load system to move with constant speed horizontally, the external force F^* must vary with time. Therefore, F^* is not a conservative force. Figure 1(*b*) shows the free body diagram of the load system. N^* is the normal force

Contributed by the Technical Committee on Vibration and Sound of ASME for publication in the JOURNAL OF VIBRATION AND ACOUSTICS. Manuscript received December 26, 2004; final manuscript received May 21, 2006. Assoc. Editor: Chin An Tan.

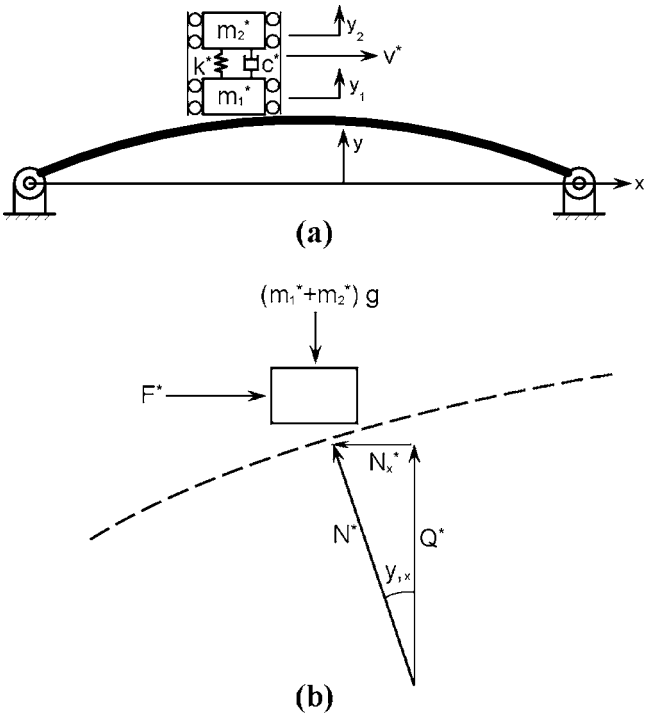

Fig. 1 (*a*) Schematic diagram of a shallow arch under a moving mass-dashpot-spring system. (*b*) The free body diagram of the load system.

acting on the load system by the arch, which can be decomposed into horizontal component N_x^* and vertical component Q^*. Since the load system moves with constant speed in the horizontal direction, the external force F^* is equal to N_x^* in magnitude, and is related to Q^* by

$$F^* = Q^* y_{,x} \tag{8}$$

Equations (1), (2), (6), and (8) can be nondimensionalized to the forms

$$u_{,\tau\tau} = -(u-u_0)_{,\xi\xi\xi\xi} + p u_{,\xi\xi} - \frac{\pi}{2} Q_g \delta(\xi - v\tau) - \frac{\pi}{2}[m_1(u_{,\tau\tau} + 2v u_{,\tau\xi} + v^2 u_{,\xi\xi}) - c(\dot{u}_2 - u_{,\tau} - v u_{,\xi}) - k(u_2 - u)]\delta(\xi - v\tau) \tag{9}$$

$$p = \frac{1}{2\pi}\int_0^\pi (u_{,\xi}^2 - u_{0,\xi}^2) d\xi, \tag{10}$$

$$m_2 \ddot{u}_2 + c(\dot{u}_2 - u_{,\tau} - v u_{,\xi}) + k(u_2 - u) = 0 \tag{11}$$

$$F = Q u_{,\xi} \tag{12}$$

where

$$(u, u_0, u_2) = \frac{1}{r}(y, y_0, y_2), \quad \xi = \frac{\pi x}{L}, \quad \varepsilon = \frac{L}{r}, \quad \tau = \frac{\pi^2 t}{L\varepsilon}\sqrt{\frac{E}{\rho}},$$

$$v = \frac{v^*\varepsilon}{\pi}\sqrt{\frac{\rho}{E}}$$

$$(m_1, m_2) = \frac{2}{\pi A \rho L}(m_1^*, m_2^*), \quad c = \frac{2c^*\varepsilon}{\pi^3 A\sqrt{\rho E}}, \quad k = \frac{2k^* L\varepsilon^2}{\pi^5 EA}$$

$$p = \frac{p^*\varepsilon^2}{\pi^2 EA}, \quad Q_g = \frac{2(m_1^* + m_2^*)g\varepsilon^3}{\pi^5 EA}, \quad Q = \frac{2Q^*\varepsilon^3}{\pi^5 EA}, \quad F = \frac{2F^*\varepsilon^2}{\pi^5 EA}$$

r is the radius of gyration of the cross section. ε is the slenderness ratio of the arch. $p=1$ corresponds to the Euler buckling load for a perfectly straight simply supported (pinned-roller) beam. $v=1$ corresponds to the speed of the flexural wave of a straight beam with wave length L. $\tau=1$ represents the period of the first bending mode of the simply-supported straight beam. Q_g is the force on the arch due to the weight of the load system. For an arch with specified physical parameters including slenderness ratio, m_1+m_2 is fixed when Q_g is specified. Physically, this simply means $Q_g^* = (m_1^* + m_2^*)g$. Take the example of an arch made of steel with $E = 2\times 10^{11}$ N/m^2, $\rho = 7860$ kg/m^3, $L = 10$ m, $\varepsilon = 1000$. For $Q_g = 40$, $m_1 + m_2$ will be equal to 1.

The initial shape of the arch before the load system is applied is assumed to be in the form

$$u_0(\xi) = h \sin \xi \tag{13}$$

h is the rise parameter of the arch. It is assumed that the shape of the loaded arch can be expanded as

$$u(\xi, \tau) = \lim_{N\to\infty} \sum_{n=1}^{N} \alpha_n(\tau) \sin n\xi \tag{14}$$

After substituting Eqs. (13) and (14) into Eqs. (9)–(11), and following a Galerkin's procedure, we obtain the equations governing α_n as

$$\ddot{\alpha}_n = -n^4\alpha_n - n^2 p\alpha_n - q_n, \quad n = 1,2,3,\ldots \tag{15}$$

$$m_2\ddot{u}_2 = \sum_{j=1}^{\infty}\{c[\dot{\alpha}_j \sin je + vj\alpha_j \cos je] + k[\alpha_j \sin je]\} - c\dot{u}_2 - ku_2 \tag{16}$$

where

$$p = \frac{1}{4}\sum_{k=1}^{\infty} k^2\alpha_k^2 - \frac{h^2}{4} \tag{17}$$

$$q_1 = Q \sin e - h, \tag{18}$$

$$q_n = Q \sin ne, \quad n = 2,3,\ldots \tag{19}$$

$$e(\tau) = v\tau \tag{20}$$

$$Q = Q_g + \sum_{j=1}^{\infty}\{m_1[\ddot{\alpha}_j \sin je + 2vj\dot{\alpha}_j \cos je - v^2 j^2 \alpha_j \sin je] + c[\dot{\alpha}_j \sin je + vj\alpha_j \cos je] + k[\alpha_j \sin je]\} - c\dot{u}_2 - ku_2 \tag{21}$$

The parameter $0 < e(\tau) < \pi$ represents the position of the load system on the arch. The overhead dot in the above equations represents differentiation with respect to τ. The initial conditions for Eqs. (15) and (16) are

$$\alpha_1(0) = h, \quad \alpha_n(0) = 0 \text{ for } n = 2,3, \quad \dot{\alpha}_n(0) = 0 \text{ for } n = 1,2,3,\ldots \tag{22}$$

$$u_2(0) = 0, \quad \dot{u}_2(0) = 0 \tag{23}$$

In the simplified case when the coupling effect between the load system and the arch is neglected, the Q in Eq. (21) is left with the constant load Q_g. This simplified case has been studied in detail by Chen and Lin [24].

Convergence Test of the Dynamic Response

We first consider the case when $m_2=0$ and the load system is left with a single mass m_1 sliding along the arch. The first question

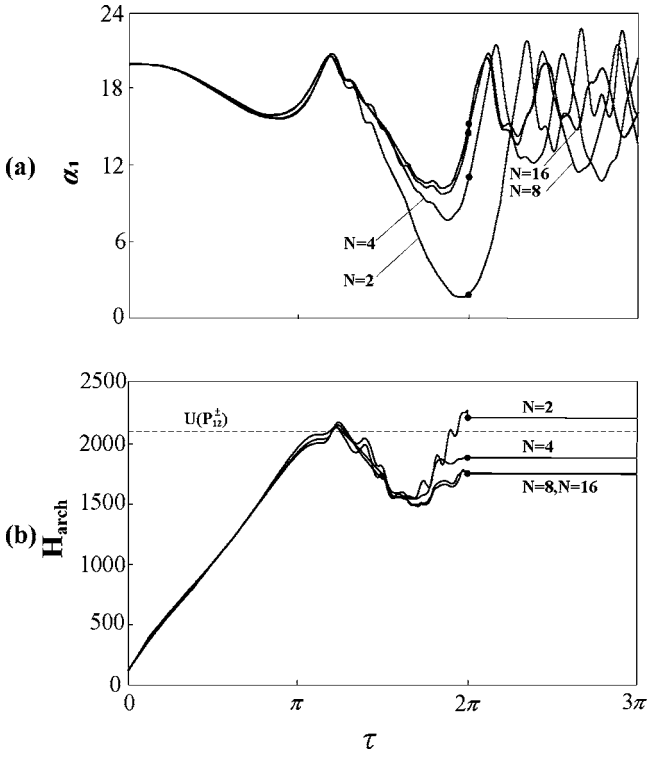

Fig. 2 Convergence test on (*a*) α_1, (*b*) H_{arch}. The parameters of the arch-mass system are $h=20$, $Q_g=40$, $\varepsilon=1000$, and $v=0.5$. The corresponding mass parameter $m_1=1$.

we have to examine is the convergence of the expansion (14). In Fig. 2(*a*) we show the response $\alpha_1(\tau)$ when 2, 4, 8, and 16 modes are used in the expansion. The arch parameters in Fig. 2(*a*) are $h=20$, $Q_g=40$, $\varepsilon=1000$, and $v=0.5$. The corresponding mass parameter m_1 is 1. In the numerical simulation we also add damping terms $\mu\dot{\alpha}_j$ in the equations of motion with $\mu=0.001$. μ represents the material damping of the arch. At the instant $\tau=2\pi$ when the point mass leaves the arch, as signified by black dots in Fig. 2(*a*), the α_1 calculated by using $N=8$ and 16 are almost indistinguishable. However, the arch continues to vibrate after the mass leaves the arch until it settles to a steady state position. As shown in Fig. 2(*a*), the responses after the mass leaves the arch can be quite different for different number of modes used even though they may be close to each other at the instant when the load system leaves the arch.

Total Energy and Energy Barrier

Although it is difficult to predict the dynamic response α_1 numerically after the point mass leaves the arch, as demonstrated in Fig. 2(*a*), it does not jeopardize our goal of establishing a more conservative condition to guarantee the safe passage of the load system without snapping the arch. We first notice that the arch may snap either while the load system is still on the arch or after the load system leaves the arch. The snapping after the load system leaves the arch can occur only if the unloaded arch has two stable equilibrium positions. Therefore, we can establish the following sufficient conditions to guarantee the safe passage of the load system as follows. (1) The total energy (the sum of kinetic energy and strain energy) gained by the arch at the instant when the load system reaches the other end is smaller than the critical energy barrier lying between the two distant stable equilibrium positions. (2) The coordinate α_1 remains greater than zero while the load system is still on the arch. Condition (1) prevents the arch from snapping after the load system leaves the arch. Condition (2) guarantees that the arch does not snap while the point load is still on the arch. The total energy H of the arch-load system can be calculated as

$$H = H_{\text{arch}} + H_{\text{load}} \tag{24}$$

where H_{arch} and H_{load} are the total energy of the arch and the load system, respectively,

$$H_{\text{arch}} = U + \sum_{n=1}^{\infty} [\dot{\alpha}_n^2] \tag{25}$$

$$H_{\text{load}} = m_1 \left\{ \left[\sum_{n=1}^{\infty} (\dot{\alpha}_n \sin n\xi + nv\alpha_n \cos n\xi) \right]^2 + 2g \sum_{n=1}^{\infty} (\alpha_n \sin n\xi) \right\} + m_2(\dot{u}_2^2 + 2gu_2) + k\left(u_2 - \sum_{n=1}^{\infty} \alpha_n \sin n\xi \right)^2 \tag{26}$$

U is the strain energy of the arch

$$U = 2p^2 + (\alpha_1 - h)^2 + \sum_{n=2}^{\infty} [n^4 \alpha_n^2] \tag{27}$$

The physical total energy H^* and strain energy U^* are related to H and U by

$$H^* = \frac{\pi^4 EI^2 H}{4AL^3}, \quad U^* = \frac{\pi^4 EI^2 U}{4AL^3} \tag{28}$$

It is noted that the kinetic energy of the load system due to the constant horizontal velocity has been neglected in Eq. (26) because it remains unchanged throughout.

The unloaded arch may admit one-mode solutions involving only α_1, and two-mode solutions involving α_1 and α_j, where $j \neq 1$. It can be shown that for $h \geqslant 4$ there are three one-mode solutions (P_0, P_1^+, P_1^-) [20]. On the other hand, there is only one one-mode solution P_0 if $h<4$. In addition, two-mode solutions $P_{1j}^{\pm}$ exist if and only if $h>2(j^2-1)(j^2-2)^{-1/2}$. Among all these one-mode and two-mode solutions, there are at most two stable ones at the same time, i.e., P_0 and P_1^-. It can be further shown that for an arch with h between 4 and $\sqrt{18}$ the critical energy barrier is the strain energy U of position P_1^+. On the other hand, for an arch with $h>\sqrt{18}$ the critical energy barrier is the strain energy of position $P_{12}^{\pm}$ [20].

The two conditions guaranteeing the safe passage of the load system can be stated mathematically as

$$H_{\text{arch}}(e=\pi) \leqslant Min[U(P_1^+), U(P_{12}^{\pm})] \tag{29}$$

$$\alpha_1(0<e<\pi)>0 \tag{30}$$

Therefore, if we can calculate the total energy H_{arch} at the instant when the load system leaves the arch accurately, we can predict whether the arch is in danger of snapping either when the load system is still on the arch or after the load system leaves the arch. Figure 2(*b*) shows the total energy $H_{\text{arch}}(\tau)$ of the arch-mass system as in Fig. 2(*a*). It is shown that the total energy calculated by using the first eight modes in the expansion converges quite well. On the other hand, using only the first two or four modes is obviously inadequate in predicting the total energy. The critical energy barrier corresponding to $U(P_{12}^{\pm})$ is also plotted as a dashed horizontal line for comparison. In particular, using only two modes in the expansion predicts that the total energy gained by the arch will exceed the energy barrier, while using more modes will predict an opposite result.

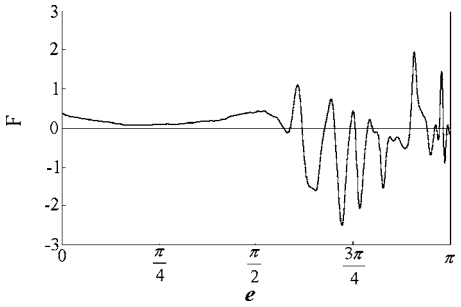

Fig. 3 External force *F* as a function of load position *e* for the arch-mass system in Fig. 2

By observing Figs. 2(*a*) and 2(*b*) we can conclude that the arch-mass system is safe from dynamic snapping. Figure 2(*a*) shows that condition (30) is satisfied, while Fig. 2(*b*) shows that condition (29) is satisfied. In summary, while eight modes are not sufficient in predicting α_1 for the physical parameter specified in Fig. 2 after the load system leaves the arch, they are sufficient in predicting whether the arch is in danger of snapping. In the following dynamic analysis, the first eight modes in the expansion are used.

Although the system under consideration is nonconservative, the conservation law of energy still holds. In other words, the work done by the external force will be equal to the total energy gained by the arch and the load system. This conservation law of energy can be used to verify the correctness of the above calculations by comparing the total energy gained by the arch-mass system with the work W done by the external horizontal force F in Eq. (12),

$$W = \int F(\tau) v d\tau \tag{31}$$

The relation between the force F and load position e for the load-mass system in Fig. 2 is shown in Fig. 3. As mentioned above in order for the load system to move with constant horizontal speed, the external horizontal force F must vary with time. The external force remains positive (pushing the mass) before the mass reaches the midpoint of the arch, while it oscillates violently in the later half of the journey. In particular, it can be negative (pulling the mass) with almost ten times of magnitude as the one in the first half of the journey. The negative horizontal force is not hard to understand. When the mass slides downhill in the second half of the journey due to gravity, it requires a negative horizontal force to slow it down in order to achieve constant horizontal speed.

After calculating the external force F, we can calculate the work in Eq. (31). It is noted that the work done by the horizontal force in the first half of the journey is positive and in the second half negative. The sum of these two parts of work is positive and is indeed equal to the total energy H gained by the arch and the load system when the load system reaches the other end of the arch. It is emphasized again that this total energy H does not include kinetic energy of the load system due to the constant horizontal velocity.

The fact that the total energy converges when eight modes are used in Fig. 2(*b*) while the α_1 response does not converge is not difficult to understand. We observe that the total energy and α_1 at the instant when the point mass leaves the arch are almost identical for $N=8$ and 16. However, for $N=16$ the total energy can spill over to the subspace α_9-α_{16} due to the nonlinear coupling among various modes, while for $N=8$ the total energy is confined to the subspace α_1-α_8. Therefore, as time goes by the α_1 in these two cases will show significant difference while the total energy in these two cases remain almost unchanged.

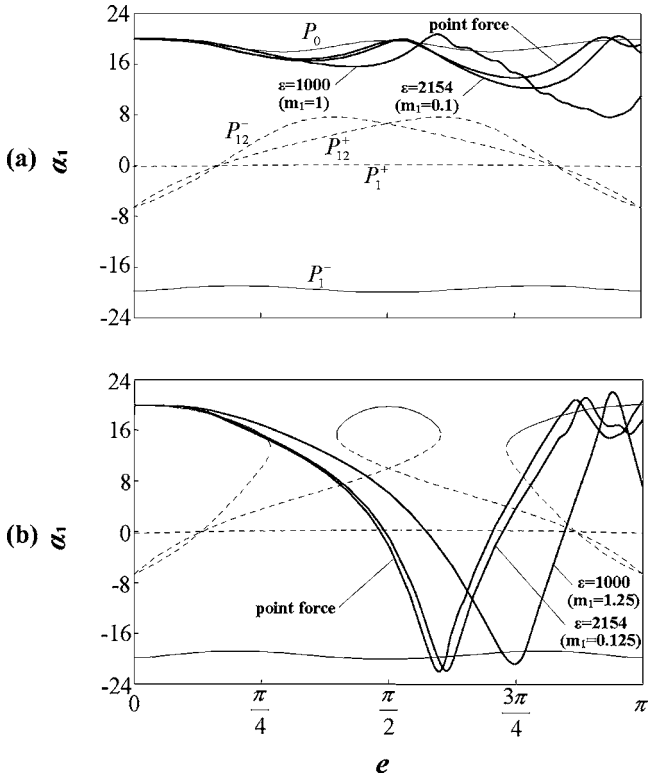

Fig. 4 Effects of slenderness ratio ε on $\alpha_1(e)$ for arches with $h=20$, $v=0.5$. (*a*) $Q_g=40$, (*b*) $Q_g=50$.

Effects of Slenderness Ratio

In this section we will examine the effects of slenderness ratio of the arch on the dynamic response. The thin lines in Figs. 4(*a*) and 4(*b*) are the equilibrium positions of the arch with $h=20$ when point loads $Q_g=40$ and 50, respectively, move on the arch quasi-statically. We use solid and dashed lines to represent stable and unstable equilibrium positions, respectively. The mode labels for one-mode solutions (P_0, P_1^+, P_1^-) and two-mode solutions $(P_{12}^{\pm})$ for the unloaded arch are retained even when the point load moves across the arch. The static critical load of an arch under a quasi-statically moving load is defined as the point load which initiates a transcritical bifurcation between the stable P_0 and the unstable P_{12}^- solutions [24]. The static critical load for an arch with $h=20$ is 47.64. Therefore, no bifurcation along the P_0 curve will occur when the point load $Q_g=40$ moves across the arch quasi-statically as in Fig. 4(*a*). Two of the three thick solid lines in Fig. 4(*a*) are $\alpha_1(e)$ calculated from the mass-only model for arches with slenderness ratios $\varepsilon=2154$ $(m_1=0.1)$ and $\varepsilon=1000$ $(m_1=1)$, respectively. The moving speed v is 0.5. The third thick solid line is the dynamic response calculated from the point-force model. The two arches in Fig. 4(*a*) do not snap dynamically while the point masses are still on the arches. Further calculation examining the total energy gained by the arches shows that they will not snap after the load system or the point load leaves the arches.

In Fig. 4(*b*) for $Q_g=50$ static snap-through occurs at $e=0.89$. Two of the three thick solid lines are the dynamic responses calculated from the mass-only model for arches with slenderness ratios $\varepsilon=2154$ $(m_1=0.125)$ and $\varepsilon=1000$ $(m_1=1.25)$, respectively. Figure 4(*b*) shows that dynamic snap-through occurs before the point mass or the point load leaves the arches.

During dynamic snap-through as demonstrated in Fig. 4(*b*), the arch experiences dramatic change in shape. The total energy of the arch-mass system contains (1) the kinetic energy of the arch, (2) the strain energy of the arch, (3) the kinetic energy of the mass m_1,

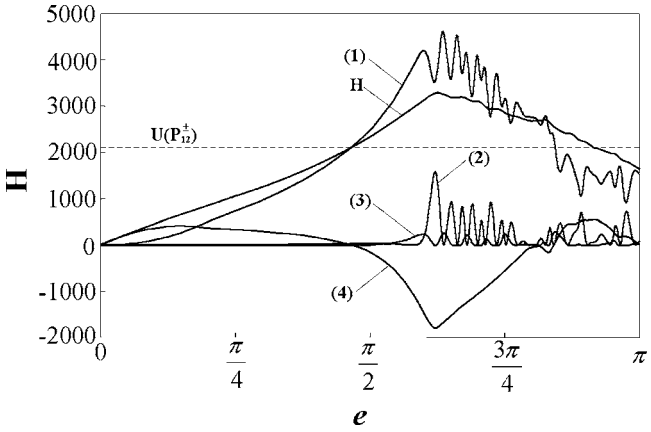

Fig. 5 Components of total energy for an arch-mass system with h=20, v=0.5, Q_g=50, and ε=2154 (m_1=0.1). (1) Kinetic energy and (2) strain energy of the arch. (3) Kinetic energy and (4) potential energy of the mass m_1.

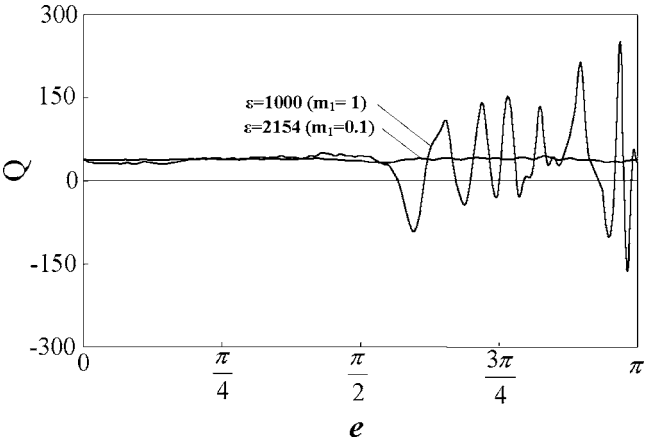

Fig. 6 Vertical component $Q(e)$ of the dynamic force applied by the load system on the arch with h=20, Q_g=40, ε=1000, and v=0.5

and (4) the potential energy of the mass m_1. In Fig. 5 we show the total energy and the above four components for an arch with h =20, Q_g=50, v=0.5, and ε=2154 (m_1=0.125). The total energy H of the arch-mass system increases monotonically in the first half of the journey, while at some point of the next half of the journey it starts to decrease. It is noted that when dynamic snap-through occurs, the strain energy and kinetic energy of the arch oscillates violently although they somewhat supplement each other. The violent oscillations of these two components are due to the excitation and growth of the higher modes in the expansion (14). In addition, the potential energy of mass m_1 also plays a significant role when dynamic snap-through occurs. The kinetic energy of mass m_1 is relatively small compared to the other three components.

From both Figs. 4(*a*) and 4(*b*), we observe that the point-force model is a good approximation when the slenderness ratio of the arch is large. As a matter of fact, in the extreme case when $\varepsilon \to \infty$, the response from the mass-only model will approach the response from the point-force model. This observation from numerical simulation can be bolstered by a simple analysis on Eq. (3). By examining Eq. (3) we expect that the point-force model should be a good approximation for the mass-only model when the acceleration term d^2y_1/dt^2 is much smaller than the acceleration of gravity g. The acceleration of the mass d^2y_1/dt^2 is proportional to the acceleration of the vibrating arch. The acceleration of the arch reaches its maximum when snap-through occurs. We can estimate the acceleration of the arch when it snaps from the very top to the very bottom with a stroke in the order of $2h$. During the snap-through action, the first mode is dominant, whose period of vibration is $(\pi^2/\varepsilon L)(\sqrt{E/\rho})$. By roughly assuming that the acceleration is constant during snap-through, we can estimate that the maximum acceleration of the mass is in the order of $4\pi^2Eh/\rho L\varepsilon^3$. This analysis confirms that the inertial force of the moving mass in Eq. (3) is negligible compared to the constant gravitational force when the slenderness ratio ε of the arch is large.

The conclusion that the point-force model is a good approximation when ε is large can also be verified by examining the vertical component Q of the dynamic force applied by the load system on the arch, as defined in Eq. (3). For the two arch-mass systems with ε=1000 and 2154 as in Fig. 2(*a*), the corresponding $Q(e)$ are shown in Fig. 6. Apparently, during the first half of the passage, the dynamic force Q agrees with the point force Q_g=40 quite well. During the latter half of the journey, on the other hand, the dynamic force Q deviates from Q_g considerably, especially for the case with ε=1000. It is noted that the force Q in Fig. 6 is related to the external force F in Fig. 3 by Eq. (12).

Effects of Moving Speed

From Eq. (9) we also expect that the inertia effect should be more significant for higher speed v. Figures 7(*a*) and 7(*b*) show the effect of different moving speeds v on the response $\alpha_1(e)$. Again Q_g in Figs. 7(*a*) and 7(*b*) are fixed at 40 and 50, respectively. The mass m_1 is fixed at 0.5. As a consequence, the slenderness ratio ε in Figs. 7(*a*) and 7(*b*) are 1000 and 1025, respectively. The responses calculated from the mass-only model and the point-force model for speeds v=0.1 and 1 are plotted in both figures. Equilibrium positions are plotted again as thin lines for comparison. For Q_g=40 in Fig. 7(*a*), the responses from the point-force model and the mass-only model are almost indistinguishable when v=0.1. On the other hand, for Q_g=50 in Fig. 7(*b*), the inertia

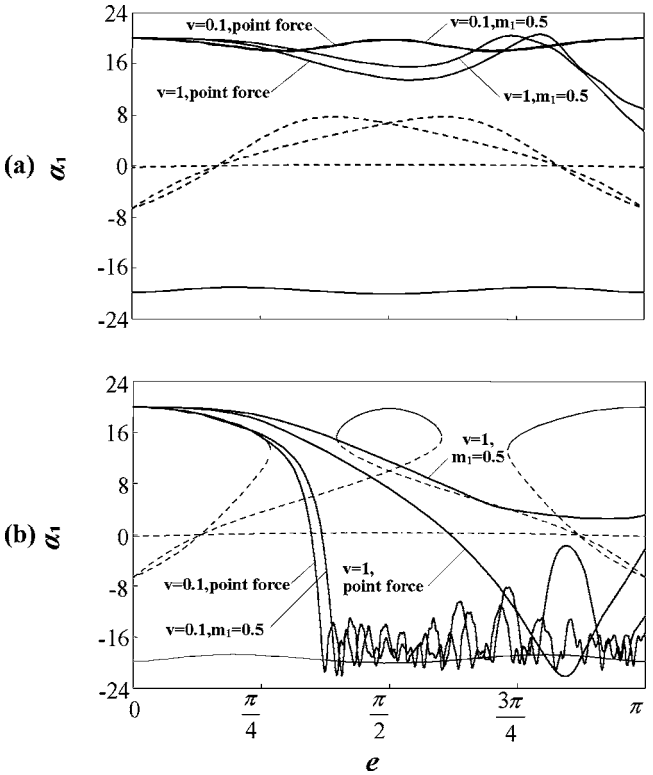

Fig. 7 Effects of moving speed v on $\alpha_1(e)$ for an arch with h =20 and m_1=0.5. (*a*) Q_g=40, (*b*) Q_g=50.

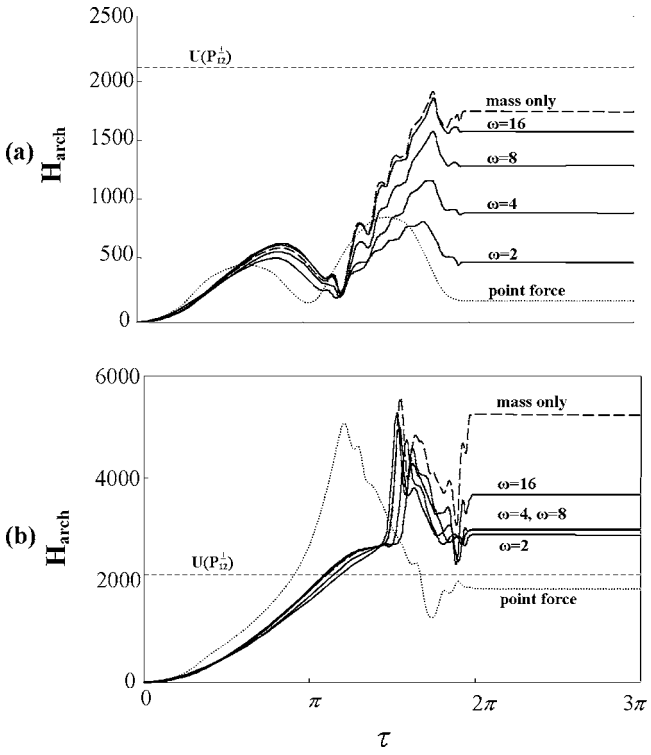

Fig. 8 Effects of suspension (with critical damping) on the total energy of the arch for $v=0.5$. (a) $Q_g=40$. (b) $Q_g=50$. Other parameters are $h=20$, $m=0.5$ ($\varepsilon=1000$).

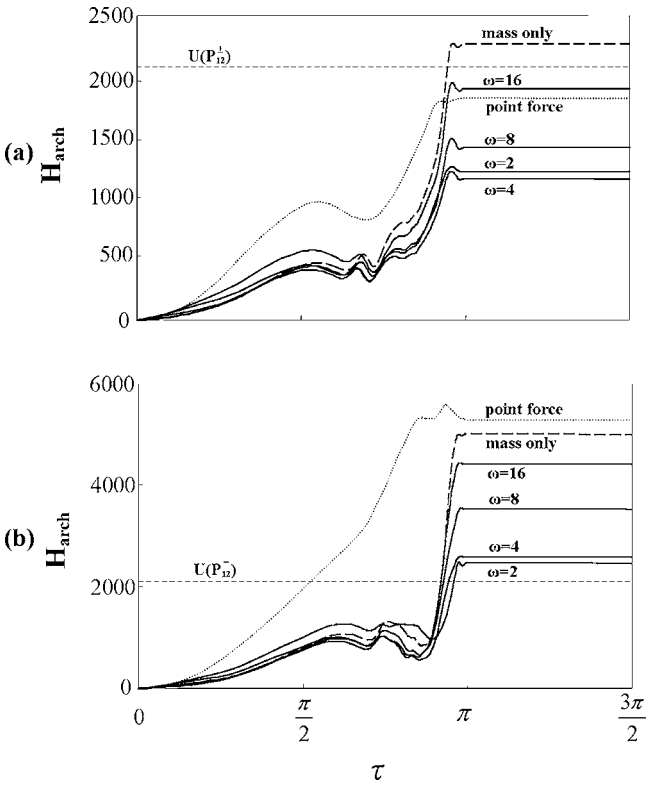

Fig. 9 Effects of suspension (with critical damping) on the total energy of the arch for $v=1$. (a) $Q_g=40$. (b) $Q_g=50$. Other parameters are $h=20$, $m=0.5$ ($\varepsilon=1000$).

effect can cause significant difference at higher speed $v=1$, with the point-force model predicting dynamic snap-through while the mass-only model predicting no dynamic snap-through before the mass leaves the arch.

Effects of Suspension

In this section we consider the complete load system with two masses connected by a suspension spring k and a dashpot c. For the special case with $m_1=m_2=m$, the natural frequency of the undamped load system is $\omega=\sqrt{k/m}$. We assume that the damping of the load system is equal to the critical damping, i.e., $c=2\sqrt{km}$, which is a reasonable design of modern vehicle. Figures 8(a) and 8(b) show the total energy $H_{\text{arch}}(\tau)$ gained by the arch for $Q_g=40$ and 50, respectively. The moving speed of the load system $v=0.5$ is relatively small. Other physical parameters are $h=20$, $m=0.5$ ($\varepsilon=1000$), and various values of spring constant. In Figs. 8(a) and 8(b) the load system leaves the arch when $\tau=2\pi$. The curves corresponding to point-force model and mass-only model are plotted by dotted and dashed lines, respectively, for comparison. The corresponding energy barriers are plotted as horizontal dashed lines. For this moving speed Figs. 8(a) and 8(b) show that the total energy gained by the arch increases as the stiffness of the suspension spring increases, with the point-force model as the lower bound and the mass-only model as the upper bound. Actually, the energy predicted when $\omega\to\infty$ should approach the energy for mass-only model. Apparently, the addition of the suspension stiffness in this speed range increases the chance of safe passage of the load system without inducing snap-through buckling.

Figures 9(a) and 9(b) are similar to Figs. 8(a) and 8(b) except that the moving speed is changed to $v=1$. For this case the load system leaves the arch when $\tau=\pi$. For this relatively high speed the simple trends observed in Figs. 8(a) and 8(b) are no longer valid. First of all, although the energy predicted by the mass-only model remains to be the upper bound, the energy predicted by the point-force model is no longer the lower bound. Second, in Fig. 9(a) the energy predicted by $\omega=2$ is greater than the energy predicted by $\omega=4$.

Dangerous Speed Zone

In Ref. [24] Chen and Lin plotted the dangerous speed zone for an arch under a point force Q moving with constant speed v. The dangerous speed zone is the parameter region in which the arch runs the risk of dynamic snap-though either when the load system is still on the arch or after the load system leaves the arch. It has been demonstrated in the preceding sections that point-force model is a good approximation for the suspension model only if the arch is slender and the moving speed is relatively low. Furthermore, the dynamic behavior of the arch becomes more complicated when a suspension is included in the load system. It is then necessary to examine the dangerous speed zone for various models. In Fig. 10 we plot the dangerous speed zone in the Q_g-v space for an arch with $h=20$ and $\varepsilon=1000$. Each Q_g corresponds to a unique value of m_1+m_2. We assume that $m_1=m_2=m$, and the spring constant $k=50$. Again the critical damping is assumed in the suspension. We divide the parameter space in Fig. 10 into 150 by 125 points. For each of these parameter points we examine conditions (29) and (30) and locate the point at which the equal sign of condition (29) is satisfied. The damping coefficient μ is chosen to be 0.001. The crosshatched area represents the dangerous speed zone with the solid line as the boundary. It appears that there are two separate regions in which dynamic snap-through might occur. It is emphasized here that for an arch-load system with the parameters within the dangerous speed zone, the arch may or may not snap. On the other hand, for those parameters not within the dangerous speed zone, it is guaranteed that it will not snap.

The similar predictions for the mass-only model and the point-force model are plotted by dashed and dotted lines for compari-

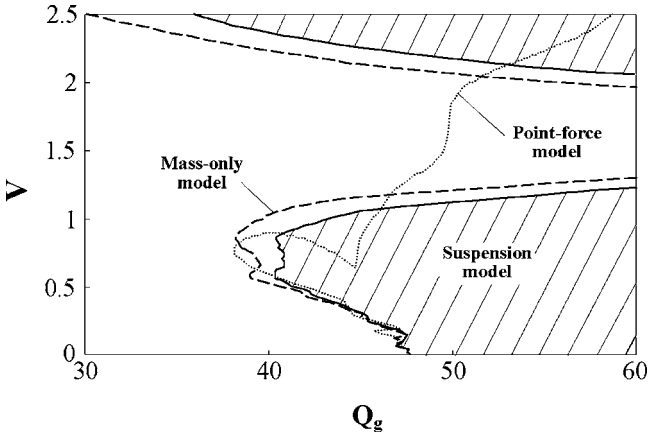

Fig. 10 The crosshatched area represents the dangerous speed zone for an arch with $h=20$ and $\mu=0.001$

son. As explained before, the mass-only model can be considered as a special case when $k \to \infty$. It appears that the mass-only model is a more conservative model compared to the suspension model as it predicts wider dangerous speed zone.

The prediction of the point-force model matches the suspension model and the mass-only model only in the lower speed region. On the other hand, the results predicted from the point-force model deviates from the predictions of the other two models considerably in the higher speed range. In particular, the point-force model predicts only one dangerous speed zone instead of two as predicted by the other two models.

Conclusions

In this paper we discuss the dynamic behavior of an arch under the action of a moving load system containing two masses, one spring and one dashpot. The load system is adopted to simulate a moving vehicle. The masses in the load system are under gravity while the gravity on the arch itself is neglected. Three different models are analyzed and compared, i.e., the point-force model, the mass-only model, and the complete suspension model. Several conclusions can be summarized as follows.

(1) It is difficult to predict accurately the dynamic response after the point load system leaves the arch no matter how many modes are used in the simulation. However, the total energy calculated by using the first few modes in the expansion converges quite well. This convergence in total energy enables us to establish a sufficient condition against dynamic snap-through of the arch.
(2) The point-force model is a good approximation of the other two more realistic models in predicting the dynamic response only when the arch is slender and the moving speed of the load system is low.
(3) For the relatively low moving speed $v=0.5$ the total energy gained by the arch increases as the stiffness of the suspension spring increases, with the point-force model as the lower bound and the mass-only model as the upper bound. As moving speed increases, however, the total energy predicted by the point-force model is no longer the lower bound.
(4) The boundary of the dangerous speed zone can be established by comparing the total energy gained by the arch and the critical energy barrier. The dangerous speed zone predicted by the point-force model matches the suspension model and the mass-only model only in the low speed range.

References

[1] Timoshenko, S. P., 1935, "Buckling of Flat Curved Bars and Slightly Curved Plates," ASME J. Appl. Mech., **2**, pp. 17–20.
[2] Fung, Y. C., and Kaplan, A., 1952, "Buckling of Low Arches or Curved Beams of Small Curvature," NACA Technical Note 2840.
[3] Gjelsvik, A., and Bonder, S. R., 1962, "The Energy Criterion and Snap Buckling of Arches," J. Engrg. Mech. Div., **88**, pp. 87–134.
[4] Onat, E. T., and Shu, L. S., 1962, "Finite Deformation of a Rigid Perfectly Plastic Arch," ASME J. Appl. Mech., **29**, pp. 549–553.
[5] Franciosi, V., Augusti, G., and Sparacio, R., 1964, "Collapse of Arches Under Repeated Loading," J. Struct. Div., **90**, pp. 165–201.
[6] Roorda, J., 1965, "Stability of Structures With Small Imperfections," J. Engrg. Mech. Div., **91**, pp. 87–106.
[7] Schreyer, H. L., and Masur, E. F., 1966, "Buckling of Shallow Arches," J. Engrg. Mech. Div., **92**, pp. 1–19.
[8] Lee, H. N., and Murphy, L. M., 1968, "Inelastic Buckling of Shallow Arches," J. Engrg. Mech. Div., **94**, pp. 225–239.
[9] Simitses, G. J., 1973, "Snapping of Low Pinned Arches on an Elastic Foundation," ASME J. Appl. Mech., **40**, pp. 741–744.
[10] Hoff, N. J., and Bruce, V. G., 1954, "Dynamic Analysis of the Buckling of Laterally Loaded Flat Arches," J. Math. Phys. (Cambridge, Mass.), **32**, pp. 276–288.
[11] Humphreys, J. S., 1966, "On Dynamic Snap Buckling of Shallow Arches," AIAA J., **4**, pp. 878–886.
[12] Lock, M. H., 1966, "The Snapping of a Shallow Sinusoidal Arch Under a Step Pressure Load," AIAA J., **4**, pp. 1249–1256.
[13] Hsu, C. S., 1967, "The Effects of Various Parameters on the Dynamic Stability of a Shallow Arch," ASME J. Appl. Mech., **34**, pp. 349–358.
[14] Hsu, C. S., 1968, "Stability of Shallow Arches Against Snap-Through Under Timewise Step Loads," ASME J. Appl. Mech., **35**, pp. 31–39.
[15] Huang, N. N., and Nachbar, W., 1968, "Dynamic Snap-Through of Imperfect Viscoelastic Shallow Arches," ASME J. Appl. Mech., **35**, pp. 289–296.
[16] Fulton, R. E., and Barton, F. W., 1971, "Dynamic Buckling of Shallow Arches," J. Engrg. Mech. Div., **97**, pp. 865–877.
[17] Lo, D. L. C., and Masur, E. F., 1976, "Dynamic Buckling of Shallow Arches," J. Engrg. Mech. Div., **102**, pp. 901–917.
[18] Johnson, E. R., and Mclvor, I. K., 1978, "The Effect of Spatial Distribution on Dynamic Snap-Through," ASME J. Appl. Mech., **45**, pp. 612–618.
[19] Gregory, W. E., Jr., and Plaut, R. H., 1982, "Dynamic Stability Boundaries for Shallow Arches," J. Engrg. Mech. Div., **108**, pp. 1036–1050.
[20] Lin, J.-S., and Chen, J.-S., 2003, "Dynamic Snap-Through of a Laterally Loaded Arch Under Prescribed End Motion," Int. J. Solids Struct., **40**, pp. 4769–4787.
[21] Chen, J.-S., and Lin, J.-S., 2004, "Effects of Prescribed End Motion on the Dynamic Stability of a Shallow Arch on an Elastic Foundation," J. Engrg. Mech. Div., **130**, pp. 359–362.
[22] Chen, J.-S., and Lin, J.-S., 2005, "Exact Critical Loads for a Pinned Half-Sine Arch Under End Couples," ASME J. Appl. Mech., **72**, pp. 147–148.
[23] Chen, J.-S., and Liao, C.-Y., 2005, "Experiment and Analysis on the Free Dynamics of a Shallow Arch After an Impact Load at the End," ASME J. Appl. Mech., **72**, pp. 54–61.
[24] Chen, J.-S., and Lin, J.-S., 2004, "Dynamic Snap-Through of a Shallow Arch Under a Moving Point Load," ASME J. Vibr. Acoust., **126**, pp. 514–519.